NAVIGATION OF THE SPACE VLBI MISSION - HALCA[1]

Tung Han You[2], Jordan Ellis[3] & Neil Mottinger[2]

In February '97, the Japanese Space Agency ISAS launched the first space VLBI satellite, HALCA, with an 8 meter diameter wire mesh antenna and radio astronomy receivers capable of observing at 1.6, 4.8, and 22 Ghz. In a 560 by 21000 km orbit with a 6 hour period and 31 degree inclination, it observes celestial radio sources in conjunction with a world wide network of ground radio telescopes as part of an international collaborative effort which includes facilities in Japan, the U.S., Canada, Australia, and Europe. JPL is providing tracking and navigation support using a dedicated subnet of 11 meter antennas as well as co-observations using the DSN 70 meter antennas.

This paper describes the spacecraft dynamics model and orbit determination strategies developed to meet the stringent trajectory accuracy requirements for generating predicts for the transfer of a stable uplink frequency to the spacecraft and for determining reconstructed orbits for delivery to the NRAO VLBI correlator and the international VLBI science community.

INTRODUCTION

Very Long Baseline Interferometry (VLBI) techniques have been extensively used from ground based radio telescopes to map celestial radio sources. The angular resolution is limited by the maximum baseline between sites, which for earth based antennas, is the diameter of the earth. Longer baselines and thus increased resolution and sensitivity can be attained by placing one of the antennas in earth orbit. In February 97 the Japanese Institute of Space and Astronautical Science (ISAS) launched the first VLBI Space Observatory Program (VSOP) satellite using the newly developed M-V launch vehicle. A second VLBI satellite, Radioastron, is scheduled to be launched by the Russian Space Agency in the year 2000. The ISAS satellite, renamed HALCA, is an 800 kg spacecraft with an 8 meter diameter

---

[1]This work was carried out at the Jet Propulsion Laboratory, California Institute of Technology, Pasadena, California under contract to National Aeronautics and Space Administration

[2]Member of Technical Staff

[3]Multi-Mission Navigation Group Supervisor

wire mesh antenna and radio astronomy receivers capable of observing radio sources at 1.6, 4.8 and 22 Ghz. HALCA was initially injected into a 200 by 21000 km orbit. Three perigee raising maneuvers placed HALCA into a 560 by 21000 km orbit with a 6 hour period and 31 degree inclination. Approximately two weeks after launch, the critical deployment of the 8 meter mesh antenna was successfully completed. Perigee, initially in the northern hemisphere for communications with the command site in Japan during the orbit transfer, precesses at a rate of 0.96 degrees per day. Communication for commanding and engineering data is at S-band (2.3 Ghz). VLBI science data and two-way Doppler are collected at Ku-band frequency (15.3 Ghz).

The Space VLBI program is an international collaborative effort which includes facilities in Japan, the U.S., Canada, Australia, and Europe. ISAS provided the spacecraft and the launch vehicle, and is responsible for operating the spacecraft and coordinating the observation sequence of the orbiting antenna with the network of tracking stations and radio telescopes. The U.S. has constructed a network of dedicated Orbiting VLBI tracking stations to support the space VLBI missions, is providing Jet Propulsion Laboratory (JPL) tracking and navigation services, co-observation with the Deep Space Network (DSN) 70-meter antennas, and correlation using facilities of National Radio Astronomy Observatory (NRAO).

The VLBI observation requires lengthy uninterrupted reception of a radio signal at the radio telescope receiving sites. During the VLBI session, uplink phase control must be maintained for the ground to spacecraft link. To satisfy this requirement for nearly continuous contact, a world wide network of five Ku-band tracking stations has been committed to supporting the mission. The DSN has constructed an Orbiting VLBI subnet of three 11 meter stations at sites in Goldstone, Madrid, and Australia. A 14 meter antenna at the NRAO Green Bank site was modified to support HALCA and a new 10 meter station was constructed by ISAS at the Japanese Usuda site. The tracking stations transfer a stable uplink reference frequency to HALCA, record the VLBI data which is downlinked in real time from the spacecraft and collect two-way Ku band Doppler for orbit determination.

This paper describes the orbit determination strategies developed at JPL to satisfy the predicts and reconstruction accuracy requirements. Orbit determination for the Space VLBI missions is unique because it involves a highly elliptic earth orbiter with relatively stringent prediction and reconstruction accuracy requirements. These requirements are dictated by the characteristics of the Ku-band tracking stations and the correlation process. The primary data type for determining the orbit is the two-way Ku-band Doppler which is generated by the reference phase transfer operation. The most challenging aspect of the strategy entailed modelling the dynamic effects due to solar pressure and drag acting on the 8 meter mesh antenna. The next section describes the source of the accuracy requirements and details of the support plan. Dynamic and observation models and estimation strategies are discussed in subsequent sections.

Predicts	
Position	170 m
Velocity	27 cm/s
Reconstruction	
Position	80 m
Velocity(22 Ghz)	0.43 cm/s
Velocity(5 Ghz)	1.9 cm/s
Acceleration(Weak Sources)	6×10^{-8} m/s^2
Phase Residual(Weak Sources)	1.2 mm
Acceleration(Routine Ops)	4×10^{-7} m/s^2
Phase Residual(Routine Ops)	14 mm

Table 1: HALCA ORBIT ACCURACY REQUIREMENTS (1 SIGMA)

MISSION SUPPORT

Navigation Accuracy Requirements

The Space VLBI missions have science and operational objectives which translate into comparatively stringent navigation requirements. A continuous uplink of a ground reference frequency is required to provide a stable reference for the on-board receiver. This signal is the source of the timing information for the VLBI data received at the spacecraft. The uplink is phase compensated to remove the effects of the uplink Doppler shift. This signal is coherently retransmitted by the spacecraft to the tracking site where a predicted downlink Doppler shift is removed to minimize the ground receiver tracking loop degradation. The phase is sampled at the tracking site 400 times per second which translates into a requirement that the error in the predicted received frequency at the spacecraft be less than 175 Hz (3 sigma).

Table 1 summarizes the (one sigma) accuracy requirements imposed by the U.S. Space VLBI project for the predicted and reconstructed orbits. Accuracies for predicted orbits are based on translating the frequency error into equivalent position and velocity errors. Position, velocity, (and acceleration) requirements are expressed as one-dimensional errors. The predicted velocity error represents the component along the tracking station to spacecraft line of sight and the predicted position error the component along the projection of the velocity vector in the plane of sky. Accuracies for reconstruction orbits are defined for the component along the direction to the observed radio source.

Requirements for the reconstructed orbit, derived by R. Linfield (Ref. 1), are governed by the the design of the VLBA correlator. The limit of 128 delay lags per frequency channel translates into an 80m (1-sigma) reconstruction requirement. The velocity error is fixed by the maximum fringe rate of the correlator. The requirement for the acceleration accuracies (Ref. 2) are expressed for routine viewing of strong and intermediate strength sources and for viewing of weak sources. The most stringent acceleration accuracies result from experiments for mapping weak sources at 5 GHz with integration times greater than 300 seconds. The acceleration error is the resulting rms error derived from fitting the phase

residuals at the correlator to a first order polynomial. The error can either be expressed as a residual (after the fit) phase error or as a one-dimensional pseudo acceleration error. The latter interpretation is based on equivalencing the second order error to an equivalent acceleration.

Since reconstruction requirements are defined by the characteristics of the VLBI correlator, the requirements are only meaningful when HALCA is observing a radio source. A minimum spacecraft altitude of 2500 km is assumed for usable VLBI data. (Reconstruction accuracy requirements imposed by ISAS are significantly less stringent ($\sim$ 800 m) due to the difference in design of ISAS correlator which processes station and spacecraft signals in separate passes.)

Navigation Operations Procedures

Extensive coordination between JPL navigation, the ISAS Mission Control Center, and the ISAS navigation center is required for orbit determination. ISAS provides JPL a sequence of events with information needed to model spacecraft dynamics, and the times of any thruster events and momentum dumps. This includes HALCA Antenna pointing angles and a schedule for radio source observations.Twice each week JPL navigation generates a 7 day predicted orbit using the Doppler data received daily from the DSN Orbiting VLBI and Green Bank stations. The predicted trajectory is delivered to the DSN and Green Bank sites. (ISAS navigation is responsible for delivering predicts to the Japanese stations.) The agencies exchange tracking data and orbit solutions weekly. Since the reconstructed orbit is delivered one week from the time of the last data point collected, tracking from all sites, including Usuda, is available for the orbit determination. Reconstructed orbits covering a seven day span are delivered in a standard portable format to the U.S. Space VLBI Project for use at the VLBI correlators.

Navigation Operation Tools

In the early stages of designing an operating system to support orbit determination, it became apparent that graphical user interfaces (GUI) were needed to simplify case setup and execution. The GUIs created enable the user to visualize the processing activities for the current week in the context of prior weeks' activities. A new case can be initialized using a designated previous case as a reference. Other data which must be updated, for example the ISAS file containing the HALCA antenna pointing angles, is acquired from the U.S. Space VLBI project. Access to three different computer platforms is provided by GUIs to gather all the data needed to setup a new case.

As data are gathered in preparation for trajectory product generation, a visualization program displays: (1) station view periods, planned tracking times, and tracking data currently available; (2) spacecraft 8-m antenna source pointing and VLBI activities; (3) the time when various trajectory events occur, e.g., periapsis, apoapsis, and eclipses. From this it is possible to easily verify that the necessary data are available. Then navigation

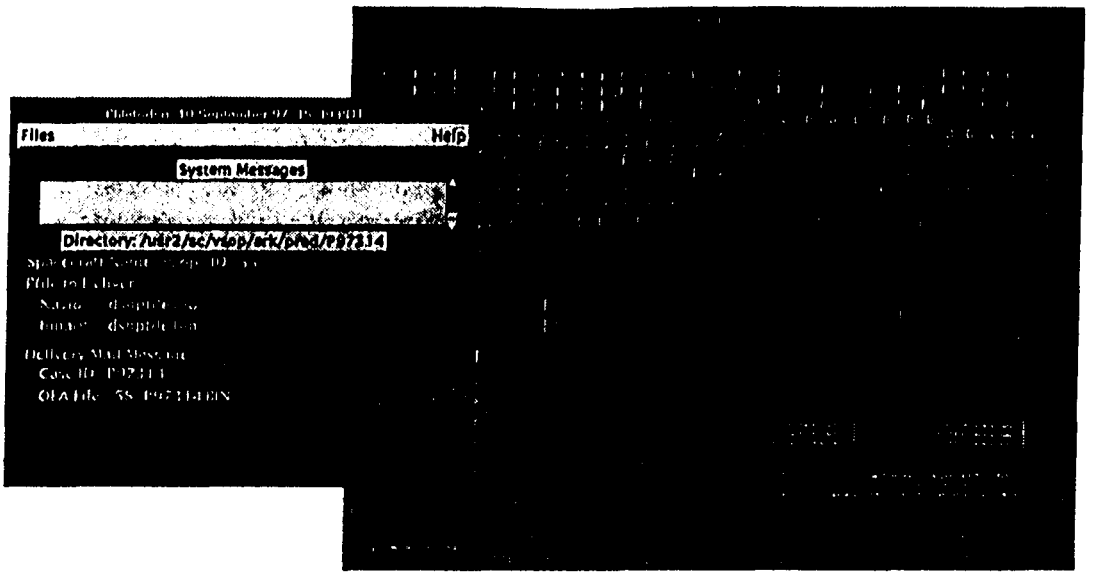

Figure 1: Examples of GUIs

software is activated through other GUIs, including a menu driven interactive data selection and display program for orbit estimation and solution validation.

When trajectory products are created, other GUIs are used to move them to the proper platform, e.g., a DSN computer for predicts generation, a U.S. Space VLBI computer for access by Green Bank, the NRAO VLBI correlator, or other members of the VLBI science community.

Overall, the GUIs have reduced the processing time by a factor of four. They provide efficient ways to gather the information needed to conduct and validate the orbit determination activities and disseminate navigation products. Figure 1 demonstrates GUIs used in HALCA operation.

MODELS FOR ORBIT DETERMINATION

Dynamic Models

The space VLBI missions are unique in that they are highly elliptic earth orbiters with relatively stringent navigation accuracy requirements for both prediction and reconstruction. Precision orbit determination requires detailed models for the spacecraft dynamics and the observations. A primary factor contributing to the orbit determination difficulty for HALCA is the uncertainty in modelling the nongravitational accelerations. This includes the effects of solar pressure force acting on the large antenna and solar panels, atmospheric drag at periapsis passage, autonomous thruster firings for transfer to and from safe hold mode, and any outgassing effects. The dominant nongravitational acceleration is expected to be the solar pressure force. Modelling this requires a measure of the effective area of

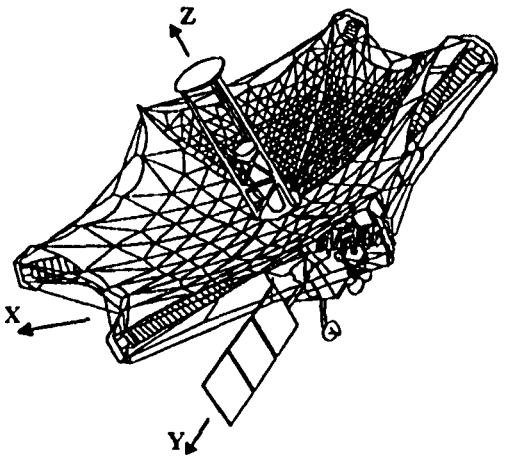

Figure 2: HALCA Structure

the "transparent" mesh VLBI antenna, knowledge of the orientation and the reflectivity properties of the antenna and other spacecraft components. Because only apriori values for these parameters were available prior to launch, our estimation strategy initially attempted to improve the values during the early phases of the mission.

JPL's Double Precision Orbit Determination Program (DPODP) (Ref. 3, 4) is used to model spacecraft dynamics and observations. The trajectory is expressed in a J2000 Solar System Barycentric Reference frame. The spacecraft dynamics models for HALCA include the following:

- central body perturbation due to the Earth and third body perturbations due to sun, moon and planets (JPL Ephemeris DE403 is the source of masses and ephemeris)
- General relativistic effects due to Earth, Sun, and Moon using Solar System Barycentric formulation
- Earth geopotential model JGM3 50 × 50 (truncated from 70 × 70)
- Solid Earth Tide Deformation
- Solar pressure acceleration modeled using antenna, solar panels, and bus components
- Atmospheric drag using a Harris Priester atmosphere

Spacecraft Component Model

The key to modelling the nongravitational accelerations due to drag and solar pressure is to decompose the complex physical structure of the HALCA spacecraft into five representative component areas. These include the 8 meter mesh antenna, solar panels, and three flat plates which are used to model the central bus. The structures are defined in an orthogonal spacecraft fixed frame as shown in Figure 2 with the antenna bore sighted along

the Z axis, and the solar panels, which rotate about the Y-axis, oriented so that the front side of the panel faces the Sun. Orientation information for the spacecraft is obtained from the radio source observing scheduling which defines the spacecraft Z direction. Approximate values of the solar pressure constants (i.e., the diffuse and spectral reflectivities) were available before launch along with an estimate of 85 to 90% antenna transparency. This estimate of the antenna transparency was revised during the early phase of mission to 65%.

The total solar radiation force, F_{solar}, experienced by spacecraft is expressed as

$$F_{solar} = (\frac{C_{sf} K_{solar}}{R_{sp}^2})(\sum_{i=1}^{5} A_i f_i(\mu_i, \nu_i, \phi_i \ldots)) \quad (1)$$

where C_{sf} is the solar flux at one AU, K_{solar} is the shadow factor, R_{sp} is the Sun-probe distance, A_i is the area of spacecraft component i, and $f_i(\mu_i, \nu_i, \phi_i \ldots)$ a collective function of specular and diffuse reflectivity coefficients, μ_i and ν_i, illumination angle ϕ_i and others (shape, i.e., flat plate or parabolic antenna) of each spacecraft component i. The effective area for each component is determined from knowledge of the spacecraft orientation. The Harris-Priester atmosphere (HP) model is used for computing the atmospheric drag force on HALCA. The total atmospheric drag force, F_{atm}, is expressed in terms of the drag coefficient C_D, the atmospheric density, ρ_{atm}, and the effective cross-sectional area $\bar{A}_i$ of spacecraft component i in the direction of the body-fixed spacecraft velocity vector $\vec{V}_{sc}$ as

$$F_{atm} = -\frac{\rho_{atm} V_{sc}^2}{2} C_D (\sum_{i=1}^{5} \bar{A}_i) \vec{V}_{sc} \quad (2)$$

Measurement Models

The Doppler observables from the dedicated DSN Orbiting VLBI stations, Green Bank, and the ISAS stations are modeled using the differenced range formulation in the DPODP. The transformation of the location of the tracking station from body fixed to inertial coordinates includes polar motion calibrations and UT1-TAI timing corrections, solid earth tides, and an earth center of mass correction. Troposphere calibrations are computed using a seasonal model. The Earth Orientation file is the source of polar motion and timing data.

Although the uplink frequency is continuously varying to compensate for the uplink Doppler shift, software at the receiving station transforms the accumulated phase data to the equivalent phase for a constant uplink frequency. Consequently, a constant uplink frequency is assumed in the computation of the Doppler shift. The Doppler is sampled every 10 seconds and compressed to 60 seconds.

ESTIMATION METHODS

Uncertainties of solar pressure, atmospheric drag, and nonspherical geopotential perturbations are the major contributors to the errors in estimating the orbit. Analysis by *Tapley et al.* (Ref. 5), demonstrated that the JGM3 gravity field significantly reduced the

Parameter	Predicted Strategy	Reconstructed Strategy	A-Priori σ
constant parameters			
epoch state			
position(km)	√	√	10^5
velocity(km/sec)	√	√	10^2
solar radiation coefficient			
μ_i	√		5×10^{-2}
ν_i	√		5×10^{-2}
atmospheric drag coefficient			
C_D	√		5×10^{0}
stochastic parameters			
stochastic acceleration			
$S/C\ X(km/sec^2)$		√	10^{-10}
$S/C\ Y(km/sec^2)$		√	10^{-10}
$S/C\ Z(km/sec^2)$		√	10^{-10}

√ *parameter is estimated*

Table 2: ESTIMATED PARAMETERS

errors due to gravity mismodelling. Use of this field reduced the errors due to the gravity mismodelling to acceptable levels, directing our attention to developing estimation strategies to reduce the mismodelling effects of solar pressure, atmospheric drag, and other small forces.

Estimation strategies to determine the HALCA orbit are based on the results of covariance studies and modelling sensitivity studies (Ref. 6-10) conducted at JPL and ISAS. The goal of the navigation task is to create simple and efficient orbit determination strategies to meet the accuracy requirements of the predicted and reconstructed trajectories. To meet these requirements, different data processing and filtering strategies were developed for orbit prediction and reconstruction.

Predicted Filter Strategy

The objective of predicted trajectory generation is to provide a trajectory which satisfies the 175 Hz (3 sigma) accuracy requirement for tracking station frequency predicts. The strategy focuses on estimating the minimum parameter set consistent with achieving valid mapping results.

A six day data arc is used with a simple single batch filter (subsequently called the *predicted filter strategy*) to estimate the spacecraft epoch state and selected solar pressure and atmospheric drag parameters (see Table 2, column 2). Values of estimated parameters are constrained to maintain "realistic" values of the dynamic constants. The new estimated values form the basis of integrating the predicted, one week trajectory. Nominally, the predicted orbit is updated twice each week and delivered to the DSN and Green Bank.

Reconstructed Filter Strategy

The objective of trajectory reconstruction is to determine the best local fit within the data arc. Reconstructed solutions are initiated using the results of the predicted filter strategy. There are several advantages gained in starting from the solution obtained by the predicted filter strategy, namely, (1) easy setup (same data arc); (2) updated dynamic models (i.e., estimates); (3) un-corrupted observables; and (4) reduced nonlinearities. Using the same data arc as the predicted filter strategy, a stochastic process can be utilized to refine the spacecraft ephemeris.

Typically, the reconstructed orbit is determined by fitting a data arc of 6 days while maintaining a two to three day overlap between the data arcs of each reconstructed orbit. Position and velocity differences in the overlapping data arcs are used as a measure of the solution accuracy. Orbit reconstruction uses a batch-sequential filter (subsequently referred to as *reconstructed filter strategy*) and smoother driven by process noise to reduce the sensitivity of orbit solutions to dynamic mismodelling effects. The reconstructed filter strategy features: (1) a six day data arc; (2) multiple three hour batches; (3) epoch state formulation; and (4) stochastic three dimensional acceleration estimation (see Table 2, column 3). A Markov first order colored noise model is used for stochastic process noise with a constant value assumed in each batch interval and a three day correlation time.

The process noise sigma, σ, can be expressed in terms of the steady state sigma, σ_{ss} , the batch length δT, and the correlation time, τ, of the form

$$\sigma = \sigma_{ss}\sqrt{1 - e^{-2\delta T/\tau}} \tag{3}$$

Optimum smoothed estimates are determined by a batch-sequential filter/smoother algorithm derived by Bierman (Ref. 11). Reconstructed orbits are delivered weekly covering the 7 day period one week earlier.

Table 2 summarizes the estimated parameters in the predicted and reconstructed filter strategies. The dynamic parameters, solar pressure and atmospheric drag coefficients are estimated as constant parameters in the predicted filter and updated later in the reconstructed filter. Typically, for a six day data arc, three hour batches and three day correlation times are used in the HALCA reconstructed filter strategy. For simplicity and efficiency, three dimensional accelerations are estimated as stochastic parameters. It has been proven that this simple design is adequate to absorb the dynamic mismodellings.

Figure 3 illustrates the iteration procedure for the correlated stochastic process. The process noise time update is performed at the end of each batch and the pseudo-epoch state $\hat{X}_k$ and the process noise (stochastic) parameters $\hat{P}_k$ are mapped to batch $(k+1)$. The smoothing coefficients (Ref. 12) $(C_W, C_X, C_P)_{k+1}$, are also generated and saved for backward smoothing. The symbol $\hat{}$ represents parameters updated with new measurements. By recursively applying the measurement updates and time updates, the square root information filter (SRIF) matrix for the last batch, n, can be obtained. Along with the

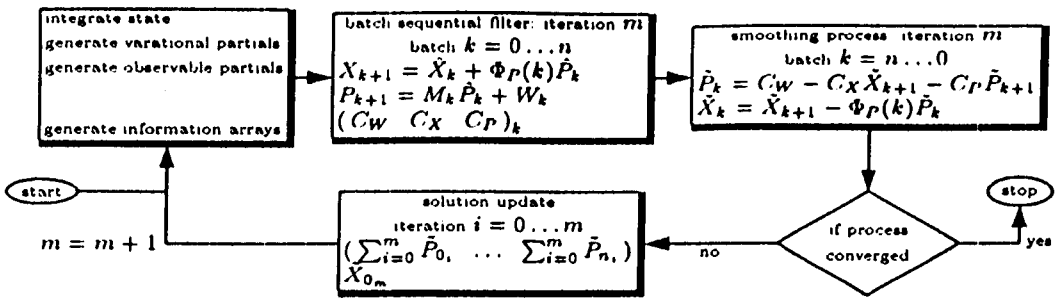

Figure 3: Stochastic Iteration Block Diagram

estimates, covariance, and smoothing coefficients, Bierman's improved Rauch-Tung-Streibel (RTS) smoothing algorithm is then applied recursively to obtain the smoothed epoch-state $\tilde{X}_0$ and smoothed process noise parameters $(\tilde{P}_0 \ \ldots \ \tilde{P}_n)$. The symbol $\tilde{}$ represents backward smoothed estimates, Φ_P is the state transition mapping matrix, M is a diagonal correlation matrix, W is filter process noise, and m is the number of stochastic iterations. Typically, convergence of the stochastic process takes three to five iterations.

NAVIGATION RESULTS

This section summarizes the orbit determination results for trajectory prediction and reconstruction activities. The performance of the estimation strategies is illustrated by plots of Doppler residuals and estimated values of selected dynamical constants. Plots of position and velocity differences during overlapping segments of reconstructed trajectories are also used as a means for evaluating the accuracy of these orbits.

Prediction Results

For the predicted strategy, constant values are estimated for the drag, C_D, and solar pressure reflectivity parameters μ_i and ν_i, for selected components. These estimates are compromised, however, due to limitations in the ability to update the effective area as the spacecraft orientation changes. Figure 4(a) plots the history of the atmospheric drag coefficient estimates, C_D, for a five month span. The secular trend may be attributed to seasonal changes. The fluctuations may be due to (1) short term atmospheric density changes, (2) compromised effective antenna transparency values as described above and/or, (3) incorrect spacecraft attitude information.

Similarly, Figure 4(b) plots the history of estimates for the solar radiation coefficient of the solar panels. The mean values of specular reflectivity coefficient is about 0.35. The spikes from the middle of September through the middle of October are caused by incorrect attitude information. The fluctuations may reflect the effective antenna area mismodelling described above.

Figure 5(a) shows typical post-fit Doppler residuals from the predicted filter strat-

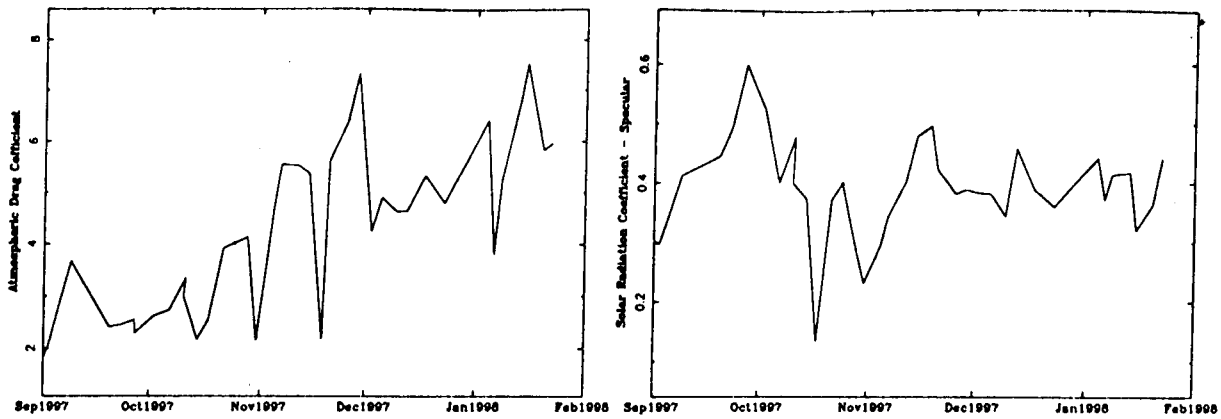

(a) *(b)*

Figure 4: Estimated Values of Atmospheric Drag Coefficient $C_D(a)$, Solar Panel Radiation Coefficient $\mu(b)$; Sep. 97 to Jan. 98

(a)

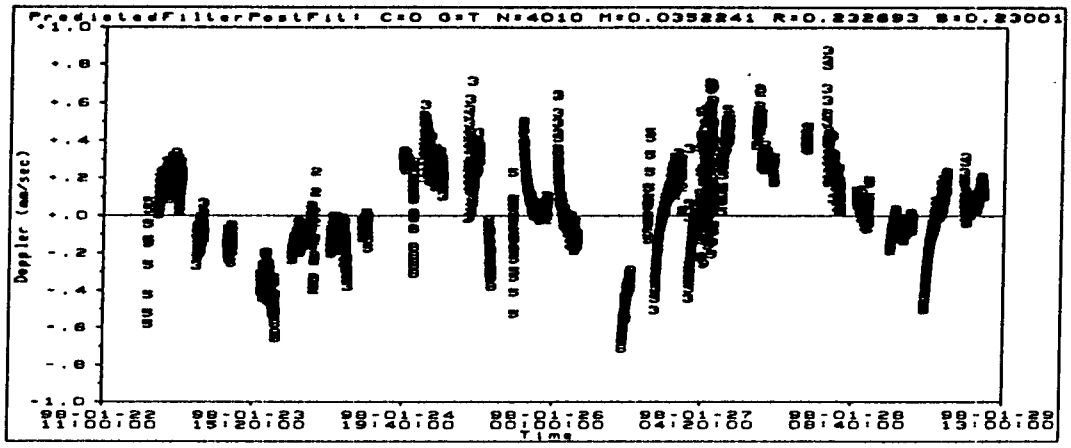

(b)

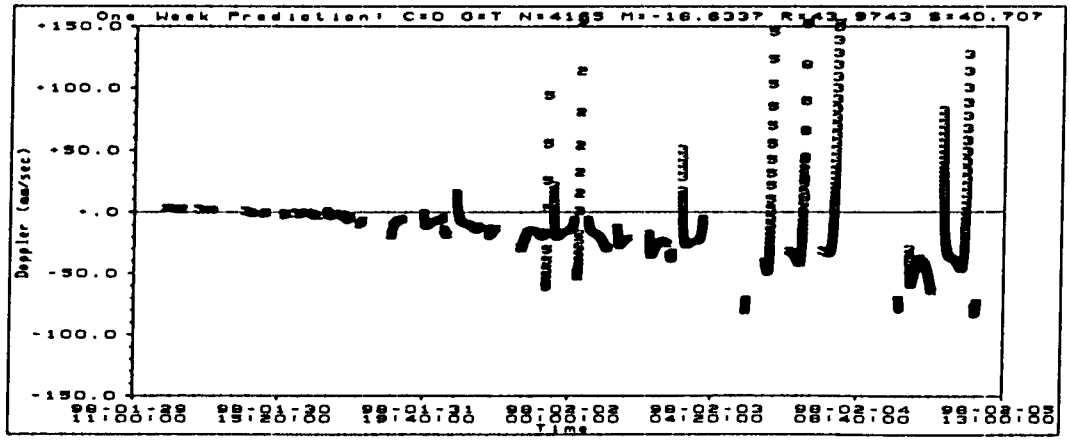

Figure 5: Predicted Filter Strategy, Ku-Band Two-Way Doppler Post-Fit Residuals(a) and One-Week Predicted Residuals(b); mm/sec

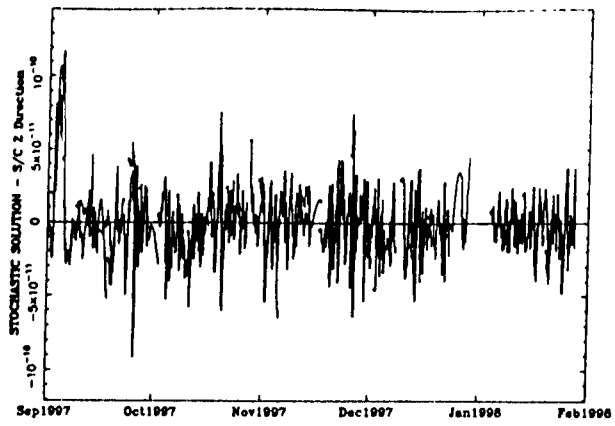

Figure 6: Estimates of Stochastic Acceleration, km/sec^2, along $S/CZ(a)$ direction; Sep. 97 to Jan. 98

egy. Tracking data is from multiple tracking stations. The data signatures imply dynamic mismodelling is still present. As discussed in previous sections, the main purpose of this strategy is not to obtain a perfect local fit, but to obtain reasonable global estimates of spacecraft constants which can be used to generate a one-week satellite ephemeris that will meet the accuracy requirements.

Figure 5(b) shows typical predicted Doppler residuals for one week. Over this span the mean residual is 80 mm/sec with the maximum deviations occurring near periapsis (for Ku-Band two-way Doppler, $1mm/sec = 0.0947hz$). The standard procedure is to update the predicts every three or four days, in which case the mean residual is about 40 mm/sec.

Reconstruction Results

To meet the more stringent orbit accuracy requirements for the reconstructed orbit, a filter strategy using stochastic processes is employed to obtain the best possible local fit. These processes are estimated as accelerations along the spacecraft Z, X, and Y directions.

The function of the stochastic processes is to absorb dynamical effects of: (1) unmodeled spacecraft orientation, particularly in the intervals when the antenna is moving from one celestial source to another; (2) mismodeled spacecraft attitude due to antenna area uncertainty and incorrect attitude information; (3) short term dynamic perturbations, especially atmospheric density fluctuations, higher order nonspherical geopotential mismodellings, and other unmodeled small accelerations. A history of stochastic acceleration is shown in Figure 6. The large initial biases present in the September 1997 estimates, were due to an interval in which there was no tracking data.

Recall that the initial setup of reconstructed filter strategy inherits the results of predicted filter strategy. For instance, Figure 5(a) shows the post-fit Doppler residuals of the predicted filter strategy and it also represents pre-fit residuals of a reconstructed case.

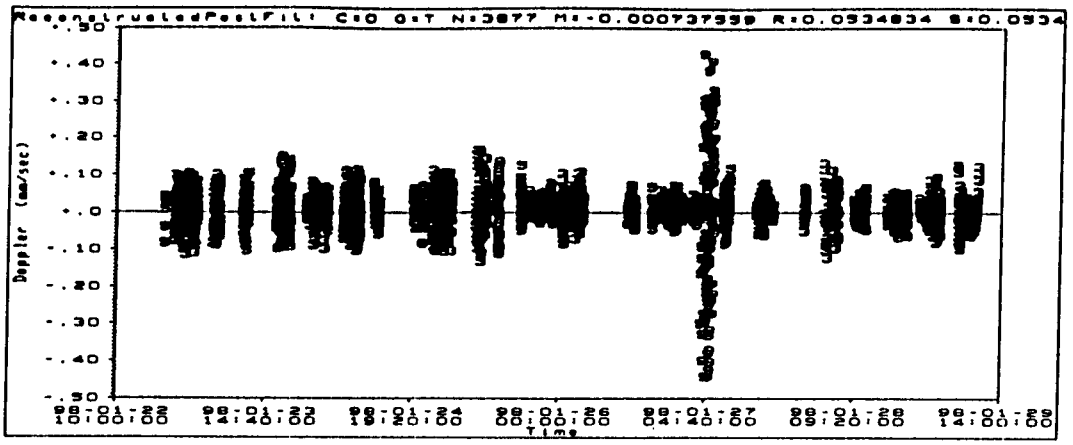

Figure 7: Reconstructed Filter Ku-Band Two-Way Doppler Residuals

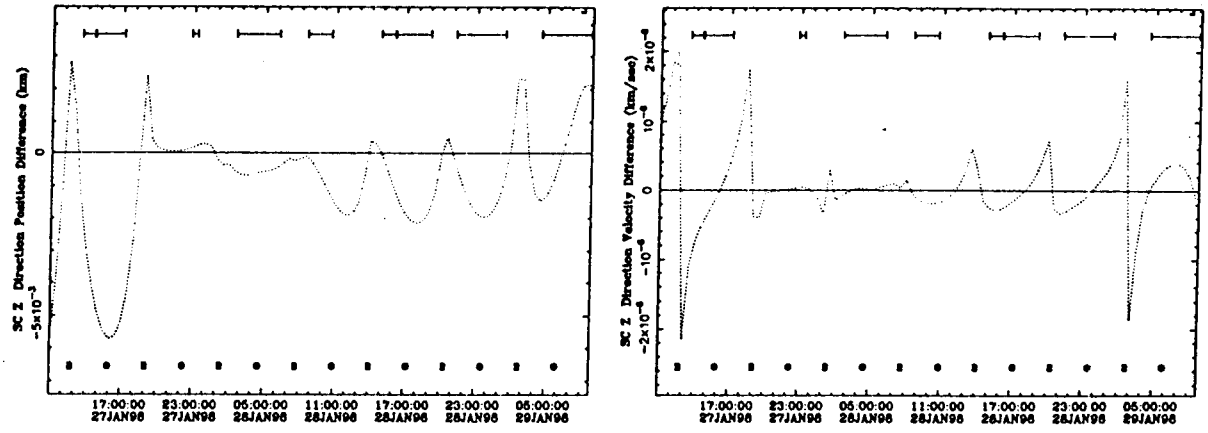

(a) *(b)*

Figure 8: Reconstructed Trajectory Relative Errors in the S/CZ direction

Figure 7 shows the post-fit reconstructed Doppler residuals for this case. Obviously, the reconstructed filter strategy has significantly improved the local fit by a factor of 5. All tracking data is compressed to 60 second count time except for the one pass with the largest data noise which is 1 second. Normally, 0.1 *mm/sec* data noise is expected for a count time of 60 seconds.

Evaluation of the reconstructed accuracy is based on differencing the overlapping segment of two reconstructed trajectories. Figure 8 shows the relative errors for a typical week. The symbol ⊢⊣ indicates spans corresponding to tracking passes and passes in which science observations are collected. The peaks in the plot correspond to periapsis and apoapsis. The maximum relative position error is 8 m and the maximum relative error is 2 *mm/sec* for this case. Recall that the accuracy requirements for 22 *Ghz* observations in position and velocity are 80 *m* and 4.3 *mm/sec* respectively. Figure 9 illustrates the history of the

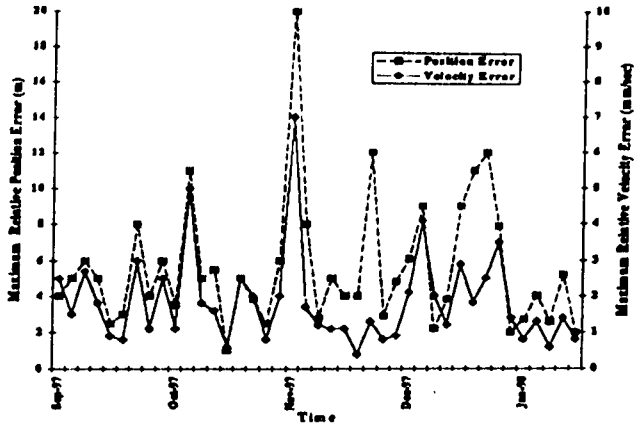

Figure 9: Maximum Reconstruction Accuracy from Sep. 97 to Jan. 98

maximum relative errors. The spikes are caused by empty batches and inconsistent attitude information.

CONCLUSIONS

HALCA is the first mission to extend VLBI techniques to incorporate an observing antenna in Earth orbit. The stringent orbit accuracy requirements for an orbiting VLBI antenna were satisfied by developing a detailed model of the spacecraft structure to model the drag and solar pressure accelerations and by developing filter strategies which reduced the sensitivity to these effects.

For orbit prediction the best strategy was determined to be a simple batch filter which estimated the spacecraft state and constrained the estimates of the solar pressure and drag parameters. For the reconstructed orbit, a batch sequential filter/smoother was required, in which stochastic accelerations were estimated in place of drag and solar pressure. The accuracy of the orbit was limited by: (1) the lack of sufficiently continuous tracking passes; (2) incorrect or incomplete knowledge of the spacecraft orientation; and (3) the absence of the data in the vicinity of perigee. The VLBI correlation process, which is very sensitive to any errors in the orbit estimates, was able to successfully utilize the reconstructed orbits to produce the expected high resolution images of the observed sources. The modeling and filtering strategies developed for HALCA are expected to be useful for application to other missions such as Russian Radioastron VLBI mission and the Space Interferometry Mission.

ACKNOWLEDGMENTS

This work was carried out at the Jet Propulsion Laboratory, California Institute of Technology, Pasadena, California under contract to the National Aeronautics and Space Administration. The authors would like to acknowledge the assistance of the U.S. Space

VLBI project and the following people in the Navigation and Flight Mechanics Section at JPL: Mark Ryne for assisting in the checkout of the DSN OVLBI Doppler subsystem; Gene Goltz, KJ Lee, Margaret Medina, Laura Campanelli, and Cheryl Stonebraker in the generation of radio metric Doppler files; Len Efron, Earl Higa, Kevin Criddle, and Kuen Wong for launch support.

REFERENCES

1. Linfield, R., "Orbit Reconstruction Requirements for VSOP and Radioastron", JPL IOM 334.6-93-001, Feb 23, 1993.
2. Linfield and J. Ulvestad, "Science Loss vs Reconstruction Orbit Acceleration Error for VSOP and Radioastron" IOM 335.1-94-018, May 27, 1993.
3. "DPTRAJ-ODP User's Reference Manual, Vol. 1", JPL Internal Document, Pasadena, CA, May 1993.
4. Moyer, T. D. "Mathematical Formulation of the Double-Precision Orbit Determination Program (DPODP)", JPL Technical Report: 32-1527, Pasadena, CA, May 1971.
5. Tapley, B.D., M. M. Watkins, J. C. Ries, G. W. Davis, R. J. Eanes, S. R. Poole, H. J. Rim, B. E. Schutz, C. K. Shum, R. S. Nerem, F. J. Lerch, J. A. Marshall, S. M. Klosko, N. K. Pavlis, and R.G. Williamson "The Joint Gravity Model 3", Journal of Geophysical Research, vol. 101, no. B12, Dec. 10, 1996.
6. Ellis, J., "Reconstructed Acceleration Errors for SVLBI Missions", IOM 314.7-290, Jun 27, 1994.
7. Ellis, J., "Navigation of Space VLBI Missions: Radioastron and VSOP", Proceedings Second International Symposium on Ground Data Systems for Space Mission Operations, JPL Pub 93-5, March1, 1993.
8. Estefan, J., "Orbit Determination of Highly Elliptical Earth Orbiters Using Improved Doppler Data-Processing Modes", TDA Progress Report 42-120, Feb 15, 1995.
9. Ichikawa, T., and T. Kato "Orbit Determination for MUSES-B Mission", ISTS Paper 94-c-21, 19th International Symposium on Space Technology, May 1994.
10. You, T. H., "VSOP Orbit Accuracy Analysis", IOM 312.C-96-003, Feb 29, 1996.
11. Bierman, G. J. *Factorization Methods for Discrete Sequential Estimation*, Academic Press, New York, NY, 1977
12. Wang, T. C., J. B. Collier, J. E. Ekelund, and P. J. Breckheimer "Applications of Square-Root Information Filtering and Smoothing in Spacecraft Orbit Determination", Proceedings of the 27th IEEE conference on Decision and Control, Vol. I, pp.825-830, Dec. 1988.